

Design and Realization of a Planar Interdigital Microsensor for Biological Medium Characterization

T.-T. Ngo, A. Bourjilat, J. Claudel, D. Kourtiche and M. Nadi

Abstract In this work, we present the design of a planar interdigital microsensor for the characterization of biological mediums by impedance spectroscopy. We propose a theoretical optimization of the geometrical parameters of this sensor. The optimization allows to extend the measurement frequency range by reducing the polarization effect which is manifested by a double layer (DL). We present also a new method for a planar interdigital transducer to determine the parameters (relative permittivity, capacitance) of the double layer (DL) on the surface of the electrode loaded by a biological medium. The CoventorWare[®] software was used to simulate the model design of interdigital transducer in three dimensions (3D). The simulation results are coherent with the method proposed. Therefore, this method can be used to determine the parameters of double layers of a planar interdigital sensor in order to match its frequency band to the intended application.

1 Introduction

Public health problems related to the electromagnetic (EM) interactions with living matter as well as therapeutical or diagnostic aims based on these interactions could take benefit from bioimpedance spectroscopy for the determination of dielectric properties of biological tissues.

It is well known that the dielectric and conductive properties of biological medium depend on frequency. However, their determination is difficult for several reasons (heterogeneity and anisotropy of tissue, difficult access, ... etc.). Biofluids for example have very complex and difficult to determine electrical properties, because of their composition and their structure. Then, using bioimpedancemetry and an equivalent electric circuit we can deduce the conductivity and the permit-

T.-T. Ngo · A. Bourjilat · J. Claudel · D. Kourtiche (✉) · M. Nadi
Institut Jean Lamour, Université de Lorraine - CNRS,
UMR 7198 Vandœuvre-lès-Nancy, France
e-mail: djilali.kourtiche@univ-lorraine.fr

tivity of the medium. Consequently, the spectroscopy of bio-impedance allows us to obtain a data bank of the values of the specific conductivity and the permittivity of biologic tissues. The bio-impedance macroscopic measurement techniques were used to characterize several organs, to characterize nerve tissues [1]. Microscopic techniques were developed since the 90s for biological cell level for the blood and the erythrocytes [2], to study suspensions of cells in the culture [3], the culture of the dependent cells of anchoring [4], etc.

Numerous structures and design of microelectrodes were developed for microscopic spectroscopy of bio-impedance. Borkholder used planar electrodes by developing his own measurement system [5]. Heushkel measured electric impedances with electrodes designed to penetrate into an *in vitro* culture of neurons [6]. Popovtzer realized a device, including eight systems of three micrometric electrodes arranged at the bottom of micro-basins [7], etc. Since the early 70s, many researchers have studied and published on sensors with planar interdigital structure for various applications like surface acoustic wave devices (SAW) [8], the design of microwave filters [9], optically controlled microwave devices [10], etc. More recently, the planar interdigital sensors were used notably in biomedical applications such as: bio-impedance Spectroscopy [11–14] and impedimetric biosensing [15], to detect *Salmonella typhimurium* [16] or *Escherichia coli* O157:H7 in food samples [17], avian influenza virus H5N1 [18], to assess different chemicals related to food poisoning [19], to study the cellular activities of B16 melanoma cell line C57BL or the flow of a fluid [20], to detect and characterize cancer cells [21], to study the humidity of the skin and the detection of the humidity of environment [22], to improve the tanning process of sheep skin to produce better quality leather [23], to determine the conductivities of near-surface material [24], electroplate materials [25], etc.

The use of the interdigital coplanar sensors gives the advantage of fast measurement process and its compatibility for a continuous operation [26]. An additional advantage is that it is also non-destructive and non-intrusive; the tested samples are not destroyed. When an electric voltage is applied to the sensor loaded by a biological medium double layer (DL) appears at the interface between the electrodes and the medium. This result on an additional interface impedance that is necessary to reduce as much as possible. For this reason, the precise determination of double layer's parameters is important in order to allow us to optimize the geometric structure of the interdigital sensor and, thus, to reduce the interface impedance.

The geometry of a sensor is one among the parameters to optimize bio-impedance measurements. Pejic [27] pointed out that the optimized structure of a sensor is one of the most crucial steps in the realization of a bio-impedance measurement device. Pejic's experiments were performed to optimize electrode design for various applications. Igraja and Dias [28] have represented new analytical expressions for the capacitance between two comb electrodes of a periodic interdigital capacitive sensor based on conformal mapping techniques. The effect of the interdigitated electrode geometry (electrode width and spacing) and electro ceramic substrate thickness on the developed strain for bulk PZT substrates was modeled by Bowen [29]. They have described in detail the optimization of interdigitated electrodes for

piezoelectric actuators and active fibre composites. Alexander [21] have optimized an interdigital sensor for impedance based evaluation of HS 578T cancer cells. Wang et al. [30] have determined the sensitivity and frequency characteristics of coplanar electrical cell–substrate impedance sensors. All these microelectrodes optimizations were made for specific applications.

In this work, we present a new approach of physical and electrical modeling system of a planar interdigital microsensor. We propose a theoretical optimization of the sensor's geometrical parameters by developing total impedance equations and modeling equivalent circuits. Furthermore, this work demonstrates a theoretical calculation to determine the relative permittivity, thickness and capacitance parameters of the double layer generated by the contact between the electrodes and the solutions. The electrical and physical models of an interdigital sensor were designed using ConvectorWare[®] software. In the following, we studied the influence of the biological medium's physical properties on the frequency sensor response. Moreover, this research also describes the correlation between the design parameters and the frequency behavior in coplanar impedance sensors.

2 Theoretical Analysis and Optimization

2.1 Basic Concepts and Definitions of the Dielectric Material

Basically, the dielectric theory is explained starting from the concept of the electrical capacitor. In a capacitor, the electrical properties of the dielectric material are maintained between two planar parallels electrodes are characterized by the capacitance (C) and the conductance (G) corresponding (see Fig. 1). When an electric voltage is applied between the electrodes, the C and the G can be determined by the following equations:

$$C = A \cdot C_0 \text{ with } C_0 = \frac{\epsilon_0 \epsilon_r}{d} \quad (1)$$

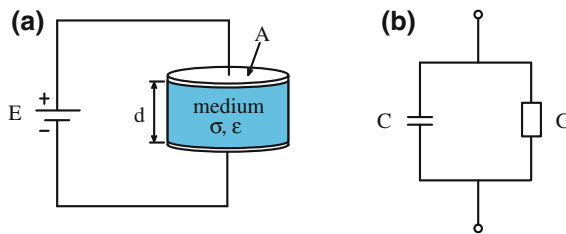


Fig. 1 **a** Dielectric biological medium between two metallic plates. **b** Equivalent circuit of a capacitor with a conductor

$$G = A \frac{\sigma}{d} \quad (2)$$

where, A is the surface of the planar electrodes (μm^2); d is the distance between the electrodes (μm); σ is the electrical conductivity of biological medium (S/m); ϵ_0 is the permittivity of vacuum and equal to $\epsilon_0 = 8.8542 \times 10^{-6}$ (pF/ μm^2); ϵ_r is the relative permittivity of biological medium; C_0 is the capacitance per unit area (pF/ μm^2).

It is well known that when a metal electrode is immersed into a biological medium, a double layer is formed at contact interface between electrode and biological medium. The determination of the parameters (relative permittivity, thickness) of double layer is necessary to obtain impedance measurement, which provides us with opportunity to calculate the relative permittivity and the electrical conductivity of biological medium. Furthermore, the capacitance per unit area (C_0) of the DL can be calculated by Eq. (1). According to Pajkossy [31] the capacitance per unit area C_0 of single crystal Pt(111) surface is similar to other metals, C_0 is approximately equal to 0.2 (pF/ μm^2).

In the work of Stern, the Gouy-Chapman model and the Helmholtz model are combined together [31–33]. Thus, the C_0 is the series combination of both capacitances ($C_{0,H}$ and $C_{0,G}$):

$$\frac{1}{C_0} = \frac{1}{C_{0,H}} + \frac{1}{C_{0,G}} \quad (3)$$

where, $C_{0,H}$ is the Helmholtz's capacitance per unit area (pF/ μm^2) and $C_{0,G}$ is the capacitance of Gouy-Chapman's model per unit area (pF/ μm^2). For most physiological systems, according to Borkholder [32], Bard and Faulkner [33], the value of $C_{0,H}$ is around 0.14 (pF/ μm^2) and $C_{0,G} = 0.07$ (pF/ μm^2). Hence, $C_0 = 0.047$ (pF/ μm^2).

2.2 Model of the Equivalent Electric Circuit

Figure 2 represents the schematic of the sensor's structure and its geometrical parameters. The equivalent electric circuit is adopted for the sensor immersed in a biological medium and is represented on Fig. 3.

Two metallic electrodes form the interdigital sensor with a comb shape, and each electrode has a width W (μm), a length L (mm) of electrodes and a distance between two consecutive electrodes S (μm). This sensor is deposited on a substrate.

The various components of biological impedance Z in this circuit is described by the electric components C_{sol} and R_{sol} . Where, the capacity of the solution is represented by the capacitance C_{sol} ; and the resistance R_{sol} describes the conductive properties of the solution under the influence of an electric field is described and is the resistance of the electrolyte solution.

Fig. 2 Geometrical structure of an interdigital sensor

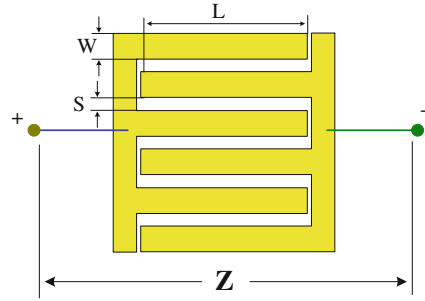
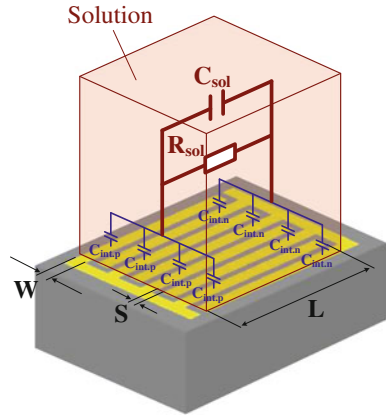


Fig. 3 Equivalent circuit model of an interdigital sensor. The C_{sol} , R_{sol} present the dielectric properties of the bio fluids, and $C_{int,p}$, $C_{int,n}$ indicate the properties of the double layer



According to Olthuis [34, 35], the R_{sol} is related to the conductivity σ_{sol} of the biological medium and the cell factor K_{cell} which depends completely on the geometry of the sensor according to the following formulas:

$$R_{sol} = \frac{K_{cell}}{\sigma_{sol}} \quad (4)$$

$$K_{cell} = \frac{2}{L(N-1)} \cdot \frac{K(k)}{K(\sqrt{1-k^2})} \quad (5)$$

where : σ_{sol} is the electric conductivity of the biological medium (S/m), N is the number of the electrodes of the sensor, L is the length of an electrode (mm), W is the width of an electrode (μm), S is the distance between two consecutive electrodes (μm), K_{cell} is the factor of cell (m^{-1}).

The function $K(k)$ is the complete elliptic integral of first kind given by the following formula:

$$K(k) = \int_0^1 \frac{1}{\sqrt{(1-t^2)(1-k^2t^2)}} dt \quad \text{where: } k = \cos\left(\frac{\pi}{2} \cdot \frac{W}{S+W}\right); \quad (6)$$

Let $\alpha = W/(S + W)$, α is the metallization ratio (for example $\alpha = 0.7$ means that 70 % metallization). Therefore, we have: $k = \cos\left(\frac{\pi}{2} \cdot \alpha\right)$.

2.3 Impedance Interface (Polarization Impedance)

In Fig. 3, the capacitance at the contact surface of each positive electrode with the biological medium is represented by the capacitance $C_{\text{int-p}}$; and the capacitance at the contact surface of a negative electrode with the solution is represented by the capacitance $C_{\text{int-n}}$. They are determined by:

$$C_{\text{int-p}} = C_{\text{int-n}} = A \cdot C_0 = LW \cdot C_0 \quad (7)$$

where, A is the surface of the each electrodes (μm^2); C_0 is the capacitance per unit area ($\text{pF}/\mu\text{m}^2$).

Since the number of negative electrodes and the number of positive electrodes are the same ($N/2$) in parallel, the total capacitance in the negative electrode and the positive electrode is calculated by:

$$\frac{N}{2} C_{\text{int-p}} = \frac{N}{2} C_{\text{int-n}} \quad (8)$$

Thus, the total capacitance at the contact surface of the sensor is determined by:

$$C_{\text{interface}} = \frac{N}{4} LWC_0 \quad (9)$$

The polarization appears at the contact surface between electrodes and solutions, it is a cause of measurement errors at low-frequency. The impedance of polarization is determined by the following expression:

$$Z_p = \frac{1}{j\omega C_{\text{interface}}} \quad (10)$$

2.4 Impedance of the Solution

We know that for a linear, homogeneous and isotropic material medium, the impedance depends not only on its electrical properties (conductivity and

permittivity), but also on the cell factor of the sensor K_{cell} [36, 37]. The impedance and the admittance are described by the following expressions:

$$\begin{cases} Z = \frac{K_{\text{cell}}}{\sigma_{\text{sol}} + j\omega\epsilon_0\epsilon_r} \\ Y = G + j\omega C \end{cases} \Rightarrow \begin{cases} G = \frac{\sigma}{\epsilon_0\epsilon_r} \\ C = \frac{K_{\text{cell}}}{K_{\text{cell}}} \end{cases} \quad (11)$$

where, j is the imaginary symbol, ω is the angular pulsation (rad/s), Z is the complex impedance (Ω), Y is the complex admittance (S), G is the conductance (S), C is the capacitance (F).

On the other hand, the total impedance and the total admittance in the equivalent electric circuit (see Fig. 3) are calculated by:

$$\begin{cases} Z = \frac{1}{\frac{1}{G_{\text{sol}} + j\omega C_{\text{sol}}} + \frac{1}{j\omega C_{\text{interface}}}} \\ Y = \frac{1}{Z} = G + j\omega C \end{cases} \quad (12)$$

By simplifying the Eq. (12), the capacitance C can be determined as presented below:

$$C = \frac{C_{\text{interface}}G_{\text{sol}}^2 + \omega^2 C_{\text{sol}}C_{\text{interface}}(C_{\text{sol}} + C_{\text{interface}})}{G_{\text{sol}}^2 + \omega^2 (C_{\text{sol}} + C_{\text{interface}})^2} \quad (13)$$

From (13), where ω is approximately zero, the value of the total capacitance (C) can be determined by:

$$\lim_{\omega \rightarrow 0} C = C_{\text{interface}} \quad (14)$$

The Eq. (15) is the result of the substitution C from (11) and $C_{\text{interface}}$ from (9) in (14):

$$\frac{\epsilon_0\epsilon_r.\text{low_frequency}}{K_{\text{cell}}} = \frac{N}{4}LWC_0 \Rightarrow C_0 = \frac{4\epsilon_0\epsilon_r.\text{low_frequency}}{NLWK_{\text{cell}}} \quad (15)$$

From the Eq. (15), we observe that the value of C_0 depends not only on the relative permittivity of the low frequency $\epsilon_r.\text{low-frequency}$, but also depends on the sensor dimensions (N , L , W and K_{cell}). Therefore, the parameters of the double layer ($\epsilon_{r\text{-DL}}$ and d_{DL}) are determined according to Fig. 4.

The relative permittivity or dielectric constant of blood at low frequency is approximately equal to 5300 decreasing around 60 at high frequency [39]. Consequently, the capacitance per unit area C_0 is determined by formula (9). The parameters of the double layer and the capacitance per unit are indicated C_0C_0 in Table 1.

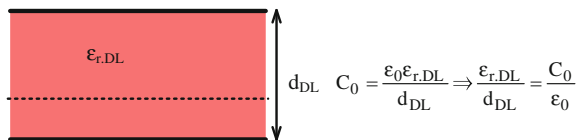


Fig. 4 Parameters of double-layer

Table 1 Parameters of interdigital sensors and DL

N	W (μm)	S (μm)	K _{cell} (m ⁻¹)	C ₀ (pF/μm ²)	ε _r · DL/d _{DL} (μm ⁻¹)
10	120	80	94.4502	8.3 × 10 ⁻⁴	93.52
12	100	66.667	77.2774	1.0 × 10 ⁻³	114.31
14	85.71	57.143	65.3886	1.2 × 10 ⁻³	135.09
16	75	50	56.6701	1.4 × 10 ⁻³	155.87
18	66.67	44.444	50.003	1.6 × 10 ⁻³	176.66
20	60	40	44.74	1.7 × 10 ⁻³	197.44
22	54.55	36.364	40.4786	1.9 × 10 ⁻³	218.22
24	50	33.333	36.9588	2.1 × 10 ⁻³	239
26	46.15	30.769	34.0021	2.3 × 10 ⁻³	259.79
28	42.86	28.571	31.4834	2.5 × 10 ⁻³	280.57
30	40	26.667	29.3121	2.7 × 10 ⁻³	301.35
32	37.5	25	27.421	2.9 × 10 ⁻³	322.14
34	35.29	23.529	25.7591	3.0 × 10 ⁻³	342.92
36	33.33	22.222	24.2872	3.2 × 10 ⁻³	363.7
38	31.58	21.053	22.9744	3.4 × 10 ⁻³	384.49
40	30	20	21.8	3.6 × 10 ⁻³	405
42	28.57	19.048	20.733	3.8 × 10 ⁻³	426.05
44	27.27	18.182	19.7686	4.0 × 10 ⁻³	446.84
46	26.09	17.391	18.89	4.1 × 10 ⁻³	467.62
48	25	16.667	18.0862	4.3 × 10 ⁻³	488.4
50	24	16	17.35	4.5 × 10 ⁻³	509

2.5 The Cut-Off Frequency

The main objective of this work is the geometrical optimization of the sensor structure to widen the cut-off frequency. This frequency at which the impedance of the solution equals the interface impedance is given by [40]:

$$f_{\text{cut}} = \frac{1}{2\pi R_{\text{sol}} C_{\text{interface}}} \quad (16)$$

In this research, we use a square structure of $L \times L$. Figures 2 and 3 describe the structure of a planar interdigital sensor. From these figures, the total width of the structure is given by:

$$L = N(W + S) - S. \quad (17)$$

Because the dimension L is much larger than S , we assume the following approximation:

$$L \approx N(W + S) \Rightarrow N = \frac{L}{W + S} \quad (18)$$

By replacing R_{sol} from the Eq. (1) equation (4), the factor K_{cell} from (5), the capacitance $C_{interface}$ from (9), N from (18) and α , the equation of cut-off frequency (16) is thus rewritten as:

$$f_{cut} = \frac{\sigma}{\pi C_0} \cdot \frac{N - 1}{L \cdot \alpha} \cdot \frac{K(\sqrt{1 - k^2})}{K(k)} \quad (19)$$

2.6 Optimization of the Geometry of Electrodes

From the formula (19), the relation between the cut-off frequency and the metallization ratio α is presented in Fig. 5 with the calculated parameters as follows: $N = 20$, $L = 2 \text{ mm}$, $\sigma = 0.7 \times 10^6 \text{ (pS/}\mu\text{m)}$.

We observe in Fig. 5, that the cut-off frequency of the sensor passes through a minimum for $\alpha = 0.6$ corresponding to the sensor with $N = 20$ electrodes. Using the

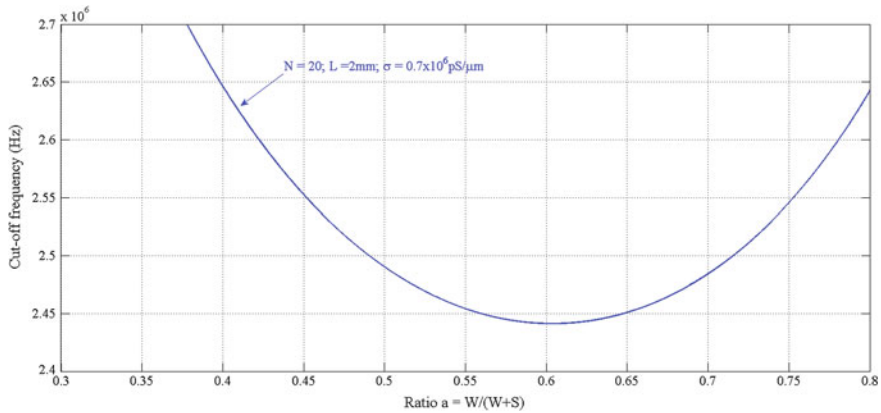


Fig. 5 Cut-off frequency of the sensor as a function of the metallization ratio α

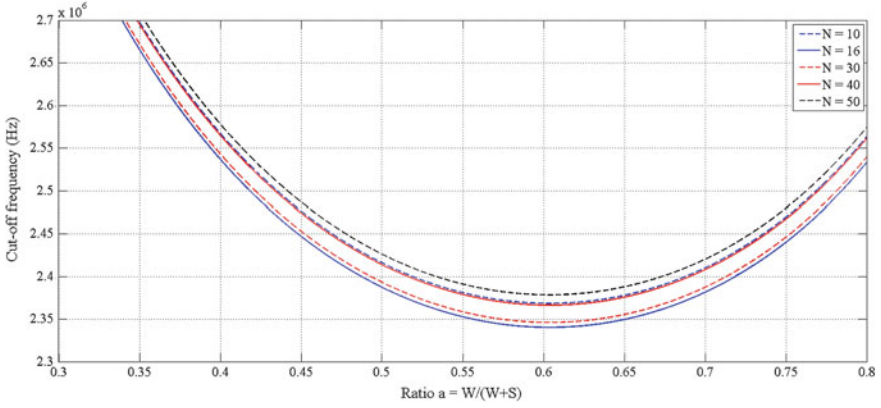


Fig. 6 Cut-off frequency of five different sensor electrodes ($N = 10, 16, 30, 40, 50$) as a function of the metallization ratio α

Table 2 Parameters of interdigital sensors and DL

N	L (mm)	$C_0(\text{pF}/\mu\text{m}^2)$
10	2	8.3×10^{-4}
16	2	1.4×10^{-3}
30	2	2.7×10^{-3}
40	2	3.6×10^{-3}
50	2	4.5×10^{-3}

relationship given above, we also study the sensors for different number of electrodes.

Figure 6 shows the cut-off frequency of different interdigitated electrodes as a function of the metallization ratio, with the calculated parameters given on Table 2.

According to Fig. 6, we see that in all cases, the number of sensor electrodes are different, the cut-off frequency always crosses through a minimum corresponding to $\alpha = 0.6$. From these results, we choose the metallization ratio $\alpha = W/(S + W) = 0.6$ as a rule to optimize the structure of the interdigitated electrodes sensor.

2.7 Optimization of the Thickness of the Biological Medium

One important parameter in bio-impedance measurement, is the thickness of the biological medium under test. Igreja and Dias [28] proposed a model for calculation of capacitance between electrodes in an interdigital sensor, based on conformal mapping techniques [41] (see Fig. 8).

where ϵ_r is the relative dielectric constant of the measured solution, $\epsilon_{r\text{-air}}$ is the relative dielectric constant of the air.

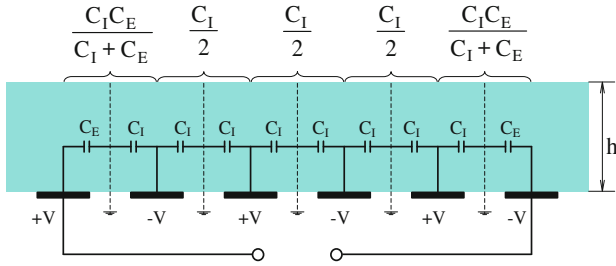


Fig. 7 Equivalent circuit for the evaluation of the capacitance with six electrodes [28]

The capacitance C_I in Fig. 7 is half the capacitance of one interior electrode relative to the ground potential and C_E is the capacitance of one outer electrode relative to the ground plane next to it. Table 3 describes the expressions used to calculate the capacitances C_I and C_E according to [25].

where,

$K(k)$ is the complete elliptic integral of first kind with modulus k

$\text{sn}(z, k)$ is the Jacobi elliptic function of modulus k

$\nu_2(0, q)$ and $\nu_3(0, q)$ are the Jacobi Theta functions

Based on the equivalent circuit of Fig. 8, where $N > 3$ one finds the total capacitance between the positive and negative electrodes by the following formula:

$$C_{\text{total}} = (N - 3) \frac{C_I}{2} + 2 \frac{C_I C_E}{C_I + C_E} \quad (20)$$

Table 3 Detailed equations needed for the calculation of C_I and C_E

Capacitance C_I	Capacitance C_E
$C_I = \epsilon_0 \epsilon_r L \cdot \frac{K(k_I)}{K(k_I')}$ $\begin{cases} k_I = t_2 \sqrt{\frac{t_4^2 - 1}{t_4^2 - t_2^2}} \\ k_I' = \sqrt{1 - k_I^2} \end{cases}$ $\begin{cases} t_2 = \text{sn}(z_2, k) \\ t_4 = \frac{1}{k} \end{cases}$ $\begin{cases} k = \left(\frac{\nu_2(0, q)}{\nu_3(0, q)} \right)^2 \\ z_2 = \alpha K(k) \end{cases}$ $\begin{cases} q = \exp(-4\pi r) \\ r = \frac{h}{\lambda} \\ \lambda = 2(W + S) \\ \alpha = \frac{W}{S + W} \end{cases}$	$C_E = \epsilon_0 \epsilon_r L \cdot \frac{K(k_E)}{K(k_E')}$ $\begin{cases} k_E = \frac{1}{t_3} \sqrt{\frac{t_4^2 - t_2^2}{t_4^2 - 1}} \\ k_E' = \sqrt{1 - k_E^2} \end{cases}$ $\begin{cases} t_3 = \cosh\left(\frac{\pi(1-\alpha)}{8r}\right) \\ t_4 = \cosh\left(\frac{\pi(1+\alpha)}{8r}\right) \end{cases}$

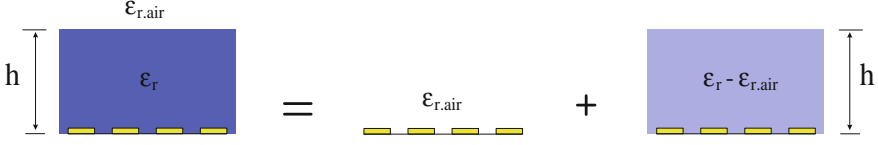


Fig. 8 Splitting of a half plane according to the partial capacitance technique

The capacitances C_I and C_E in Fig. 7, they can also be determined for a planar interdigital sensor having one or more layers (of different permittivities and thickness) on the top of the electrodes.

The capacitance of a sensor taking into account the different layers is the sum of the partial capacitances as follows:

$$C_{\text{total}} = C_{\text{air}} + C_h + C_s \quad (21)$$

where, C_{total} is the total capacitance of the upper half plane and C_h is the geometric capacitance of the measurement layer, which depends on its height h and on the particular electrode geometry and C_s is the capacitance of the substrate.

Using the equations in Table 3 and the technique of partial capacity, we obtain the total capacitances $C_{I\text{-total}}$ and $C_{E\text{-total}}$ by the following expressions:

$$\Rightarrow \begin{cases} C_{I\text{-total}} = \epsilon_0 \epsilon_{\text{air}} \cdot L \cdot \frac{K(k_{I\infty})}{K(k'_{I\infty})} + \epsilon_0 (\epsilon_r - \epsilon_{\text{air}}) \cdot L \cdot \frac{K(k_{I,h})}{K(k'_{I,h})} + \epsilon_0 \epsilon_s \cdot L \cdot \frac{K(k_{I\infty})}{K(k'_{I\infty})} \\ C_{E\text{-total}} = \epsilon_0 \epsilon_{\text{air}} \cdot L \cdot \frac{K(k_{E\infty})}{K(k'_{E\infty})} + \epsilon_0 (\epsilon_r - \epsilon_{\text{air}}) \cdot L \cdot \frac{K(k_{E,h})}{K(k'_{E,h})} + \epsilon_0 \epsilon_s \cdot L \cdot \frac{K(k_{E\infty})}{K(k'_{E\infty})} \end{cases}$$

with: $\begin{cases} k_{I\infty} = \sin\left(\frac{\pi}{2}\alpha\right) \\ k_{E\infty} = \frac{2\sqrt{\alpha}}{1+\alpha} \end{cases}$

Finally, the total capacitance of the planar interdigital sensors is given by:

$$C_{\text{total}} = (N-3) \frac{C_{I\text{-total}}}{2} + 2 \frac{C_{I\text{-total}} \cdot C_{E\text{-total}}}{C_{I\text{-total}} + C_{E\text{-total}}} \quad (22)$$

As analyzed above, we apply the Eqs. (21) and (22) to optimize the thickness h of the biological medium for planar interdigital sensors with a glass substrate. The solution under test and glass substrate have the relative permittivities: $\epsilon_r = 80$ and $\epsilon_s = 5.4$, respectively.

Figure 9 shows the relationship between the total capacitance of the planar interdigital sensors and the thickness h of the biological medium by two sensors optimized: sensor 1 and sensor 2. According to this figure, we see that the values of the total capacitance C_{total} very greatly for the thickness $h < 100 \mu\text{m}$. Then, these values do not change for a thickness greater than $100 \mu\text{m}$.

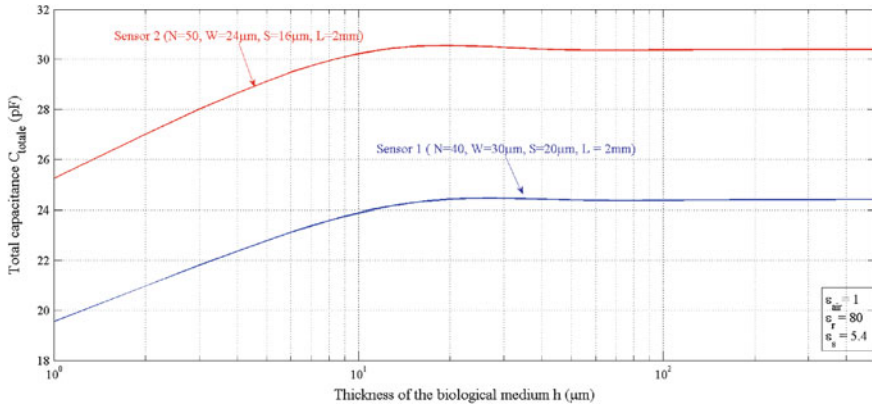


Fig. 9 The total capacitance as a function of the thickness of the biological medium

Figure 10 represents the relationship between the total capacitance of the sensor 1 and the thickness h of the biological medium by the two biological medium having different permittivities: $\epsilon_r = 80$ and $\epsilon_r = 84$.

According to this figure, we see that the values of the total capacitance C_{total} vary greatly for the thickness $h < 100 \mu\text{m}$. Then, again for the thickness $h > 100 \mu\text{m}$ these values are almost constant.

We can conclude, by analyzing Figs. 9 and 10, the thickness of the biological sample influences largely the results of the measured bioimpedance. Thus, when we measure the bio-impedance, it is necessary to have a medium thickness h greater than $100 \mu\text{m}$.

Consequently, we can choose the thickness of the biological sample as an optimization theory for the measuring bio-impedance.

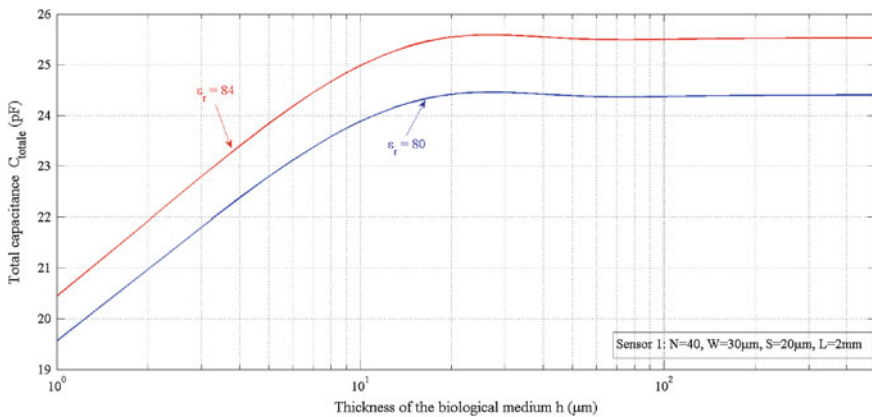


Fig. 10 Total capacitance as a function of the thickness of the biological medium

3 Simulation and the 3D Modelling of the System by Coventorware® Software

CoventorWare® is an integrated suite of software tools for designing and simulating MicroElectroMechanical Systems (MEMS) and microfluidics devices. CoventorWare supports two distinct design flows, as shown in Fig. 11, which may be used separately or in combination. The ARCHITECT module provides a unique system-level approach to MEMS design, whereas the DESIGNER and ANALYZER modules work together to provide a more conventional physical design flow. Both design flows require information about the fabrication process as a starting point, and this information is provided via a Process Editor and the Material Properties Database [42].

In this section, we describe the design of the physical model of the sensor loaded by a biological medium (for example the blood). We used the MEMS electro-quasistatic module proposed by the library of this software. In this simulation, we use the structure of the sensor at the micrometric scale. A top view is shown in Fig. 12.

3.1 Modeling of Substrate

The substrate is a glass layer of a $5000 \times 5000 \mu\text{m}$ square shape and a thickness of $1000 \mu\text{m}$.

The glass is very good insulator with a conductivity of approximately $10^{-17} \text{ S m}^{-1}$ and a permittivity very small around 5–7. Thus, we do not need to put an insulating layer between the substrate and the electrodes of the sensor.

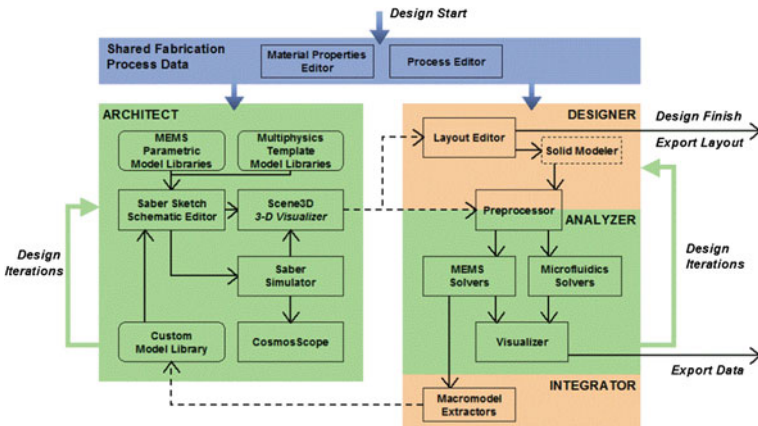
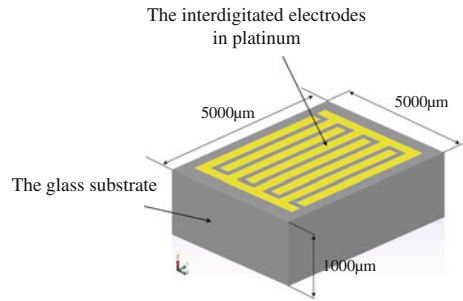


Fig. 11 Design flow [41]

Fig. 12 Model of a coplanar interdigitated electrode sensor



3.2 Modeling of Electrodes

Figure 12 describes the structure of the sensor. It is formed by two metallic electrodes in a comb shape. In the simulation, we chose the mask electrodes of platinum with a thickness of $1\ \mu\text{m}$ deposited on the substrate. The total surface occupied by electrodes corresponds to that of a square with $L = 2000\ \mu\text{m}$. The geometrical parameters of this sensor include the width of electrode W , the length of electrode L , the distance between two consecutive electrodes S and the number of electrodes N represented on Fig. 2. The platinum is one of the best materials to fabricate a sensor with interdigitated electrodes, its conductivity being of $9.66 \times 10^6\ \text{S/m}$.

3.3 Modeling of the Double Layer

As presented above, when electrodes in metal are loaded by a biological medium, a double layer is formed at their contact interface. In Fig. 3, $C_{\text{int-p}}$, $C_{\text{int-n}}$ model the properties of the phenomena of the double layer on the surface in contact between electrodes and biological medium. In Fig. 14, this double layer is presented by the layer 3.

The parameters (relative permittivity, thickness) of double layer are determined in a section above (see Table 1). For example, for the sensor forming $N = 50$ electrodes, the width of electrode $W = 24\ \mu\text{m}$, the length of electrode $L = 2000\ \mu\text{m}$, the distance between two consecutive electrodes $S = 16\ \mu\text{m}$, from the report of choose $\epsilon_{\text{r-DL}}/d_{\text{DL}} = 509\ \mu\text{m}^{-1}$, one can choose $\epsilon_{\text{r-DL}} = 590$ and $d_{\text{DL}} = 1\ \mu\text{m}$. The choice of these values do not affect the results of the simulation because the ratio $\epsilon_{\text{r-DL}}/d_{\text{DL}} = 509\ \mu\text{m}^{-1}$ is always constant.

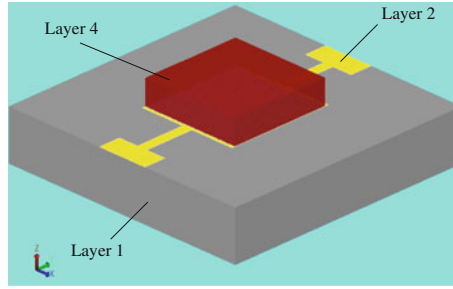


Fig. 13 The modeling 3D with CoventorWare[®], the layer 1 indicates the glass substrate, the layer 2 represents the interdigitated electrodes in platinum, and the layer 4 represents the biological medium

3.4 Modeling of the Biological Medium

The layer 4 in Figs. 13 and 14 models the electric properties of the biological solution. The thickness of this layer is equal to 500 μm , it follows the theory of optimization in the section above (the thickness h of the biological solution must be greater than 100 μm). The values of the conductivity and permittivity of human tissue is taken from [38] or [39]. For example, the conductivity of the blood of 0.7 S/m; the relative permittivity of blood at low frequency is approximately equal to 5300 at high frequency and is 60 [38] in the frequency range $10 \div 10^9$ Hz.

3.5 Simulation and Results Obtained

3.5.1 Process Simulation

According to the simulation steps mentioned above, after choosing materials, designed 2D sensor geometry and created a 3D model, we make the meshing

Fig. 14 3D view, zoomed from Fig. 13, the layer 3 describes the double layer DL

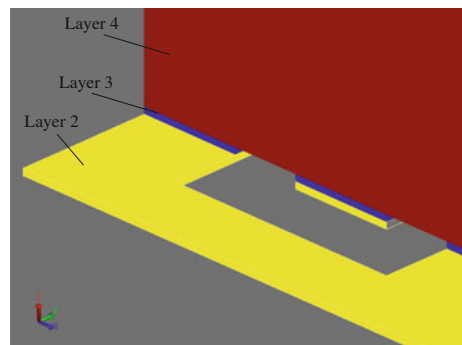
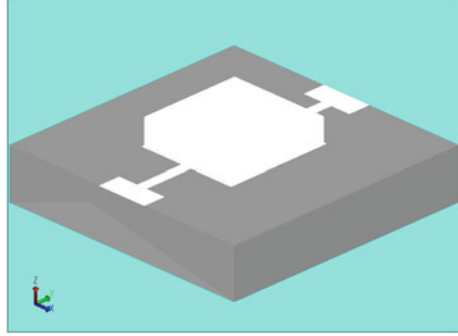


Fig. 15 3D view, the meshing of Manhattan bricks 1 μm



process. The meshing is created by using bricks of Manhattan of linear elements of 1 μm in the directions X, Y, Z. If the analysis of simulation does not converge, the mesh size is increased to 1 μm and the process of simulation starts. Figure 15 presents bricks of Manhattan of linear elements.

After meshing, a sinusoidal voltage 1 V is applied between the positive and negative electrodes. The frequency range of $10 \div 10^9$ Hz is used for the simulation.

As indicated in Fig. 11, from the analyzing by a simulation software, the available data are the results of capacitance C, conductance G between positive and negative electrodes, and the range of frequencies f. From these data, one can determine the measured quantities (the admittance Y, the impedance Z) following:

$$\begin{cases} \omega = 2\pi f \\ Y = G + j\omega C \\ Z = \frac{1}{Y} \end{cases} \quad (23)$$

From the impedance Z given in (23), the conductivity and the permittivity values of the biological research are calculated by the following expressions:

$$Z = \frac{K_{\text{cell}}}{\sigma + j\omega\epsilon_0\epsilon_r} \Rightarrow \sigma + j\omega\epsilon_0\epsilon_r = \frac{K_{\text{cell}}}{Z} \Rightarrow \begin{cases} \sigma = \text{Re}\left(\frac{K_{\text{cell}}}{Z}\right) \\ \epsilon_r = \frac{\text{Im}\left(\frac{K_{\text{cell}}}{Z}\right)}{\omega\epsilon_0} \end{cases} \quad (24)$$

where: j is the imaginary symbol, ω is the angular pulsation (rad/s), ϵ_0 is the permittivity of vacuum, ϵ_r is the relative permittivity of the biological medium, Z is the complex impedance (Ω); Y is the complex admittance (S), G is the conductance (S), C is the capacitance (F), K_{cell} is the cell factor of the sensor.

Table 4 Parameters of double layer

Authors	C_0 (pF/ μm^2)	$\epsilon_r \cdot \text{DL}/d_{\text{DL}}$ (μm^{-1})
Pajkossy [1]	0.2	22588
Borkholder [2], Bard and Faulkner [3]	0.047	5308
Our results	3.6×10^{-3}	405

3.6 Results

3.6.1 Determination of the Parameters of Double Layer

In the previous section, we have mentioned that the value of capacitance per unit area C_0 do not only depend on the relative permittivity of the medium, but also on the dimensions (geometry) of the sensor (N , L , W and K_{cell}).

According to Pajkossy [31], Borkholder [32] and Bard et Faulkner [33], the value of C_0 is constant and is presented in Table 1.

We choose different interdigitated electrodes sensor for simulations and comparisons with other authors. We choose an optimized sensor with $N = 40$, $W = 30 \mu\text{m}$, $= 20 \mu\text{m}$, $K_{\text{cell}} = 21.8 \text{ m}^{-1}$ and the value of capacitance per unit area $C_0 = 3.6 \times 10^{-3} \text{ pF}/\mu\text{m}$.

From the capacitance per unit area, we can determine the ratio between the relative permittivity and the thickness of double layer. This ratio is shown in Table 4.

The simulation for these three different cases are presented in Fig. 16. Figure 16 shows the relative permittivity as a function of the frequency. In this figure, the curve of the relative permittivity is more similar to the curve obtained in [39]. The result of blood’s relative permittivity is approximately equal to 5260 at low frequency and 65 at the high frequency. This confirms that the proposed

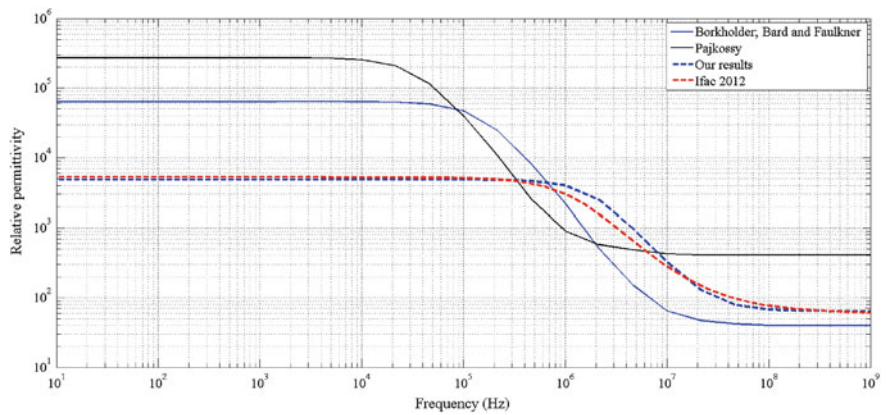


Fig. 16 Relative permittivity of blood as a function of the frequency

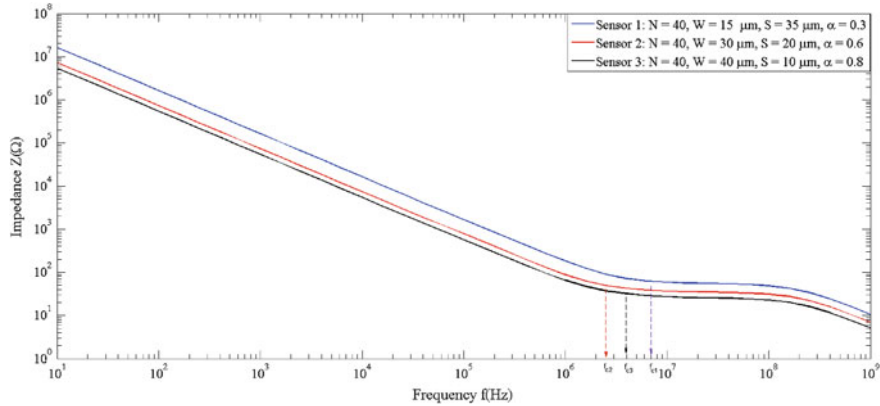


Fig. 17 Impedance as a function of the frequency

method to determine the parameters of the double layer of a planar interdigital sensor is correct.

3.6.2 Optimization of the Metallization Ratio

Figures 5 and 6 presented the relation between the cut-off frequency and the metallization ratio α . According to these figures, the cut-off frequency always crosses through a minimum corresponding to $\alpha = 0.6$ in all cases of the sensor’s different electrodes. Thus, the main result of this simulation is to check the metallization ratio. In the following we study the influence of this ratio by impedance spectroscopy.

A sinusoidal signal (1 volt) is applied between the terminals of interdigitated electrodes for 10 Hz to 1 GHz frequency range. We used the Manhattan mesh for this physical model with linear elements 10 microns of size in three directions (X, Y, and Z). The model is presented in Fig. 15.

In Fig. 17, we present the simulation results of the impedance as a function of the frequency for three types of sensors ($\alpha = 0.3$, $\alpha = 0.6$ and $\alpha = 0.8$). One must notice that the volume of the medium in all the simulation cases is the same. The geometrical parameters of the sensor used to make the simulation are given on Table 5.

The results indicated in Fig. 17 and Table 6 shows that the sensor 2 with a metal ratio of

$\alpha = 0.6$ has the lowest cutoff frequency confirm in also our theoretical approach.

Thickness of the Biological Medium Sample

Using bioimpedance spectroscopy we have determined the better thickness of the biological medium, which governs directly the quality of the measurement. From

Table 5 Simulation parameters of the interdigital sensor

Sensor	L (mm)	N	W (μm)	S (μm)	α	K_{cell} (m ⁻¹)	C_0 (pF/μm ²)	$\epsilon_{r,\text{DL}}$	d_{DL} (μm)
1	2	40	15	35	0.3	35.8	4.37×10^{-3}	493.5	1
2	2	40	30	20	0.6	21.8	3.6×10^{-3}	405	1
3	2	40	40	10	0.8	15.1	3.9×10^{-3}	438.74	1

Table 6 Results of the simulation of the cut-off frequency for three cases

Sensor	L (mm)	N	W (μm)	S (μm)	α	f_{cut} (Hz)
1	2	40	15	35	0.3	7×10^6
2	2	40	30	20	0.6	2.5×10^6
3	2	40	40	10	0.8	4×10^6

analysis of Fig. 9 and Fig. 10, one can see, as previously shown theoretically, that the thickness h of the biological sample must be greater than 100 μm.

In this section, we simulate an optimized sensor measuring a biological sample (blood) for various thicknesses. The thickness values of the biological sample under test are: 20, 40, 100, and 300 μm respectively. The sensor is formed by $N = 40$ electrodes; $\alpha = 0.6$; $L = 2$ mm; $W = 30$ μm; $S = 20$ μm.

Figure 18 shows the relation between the measurement impedance and the thickness h of the biological sample. According to this figure, one can observe that the impedance decreases when the thickness h of the biological sample increases. However the impedance do not decrease and remains constant over 100 μm.

Figure 19 shows the relation between the total capacitance and the thickness h of the biological sample for the same conditions as for Fig. 18. We can see that the total capacitance increases when the thickness h increases. And again, this increase stop for 100 μm.

These results are entirely consistent with the proposed theory for choosing the best thickness of a biological medium sample to put on the sensor.

4 Design and Realization of Micro Sensors

The realization of our interdigital sensors, was made in association with and by the competence center MINALOR of the Institut Jean Lamour (IJL) of the University of Lorraine. To study empirically the various geometries of interdigitated structures, in order to verify the optimization theory developed, five geometries of different electrodes were realized. The geometric parameters of the sensor manufacturing are described in Table 7.

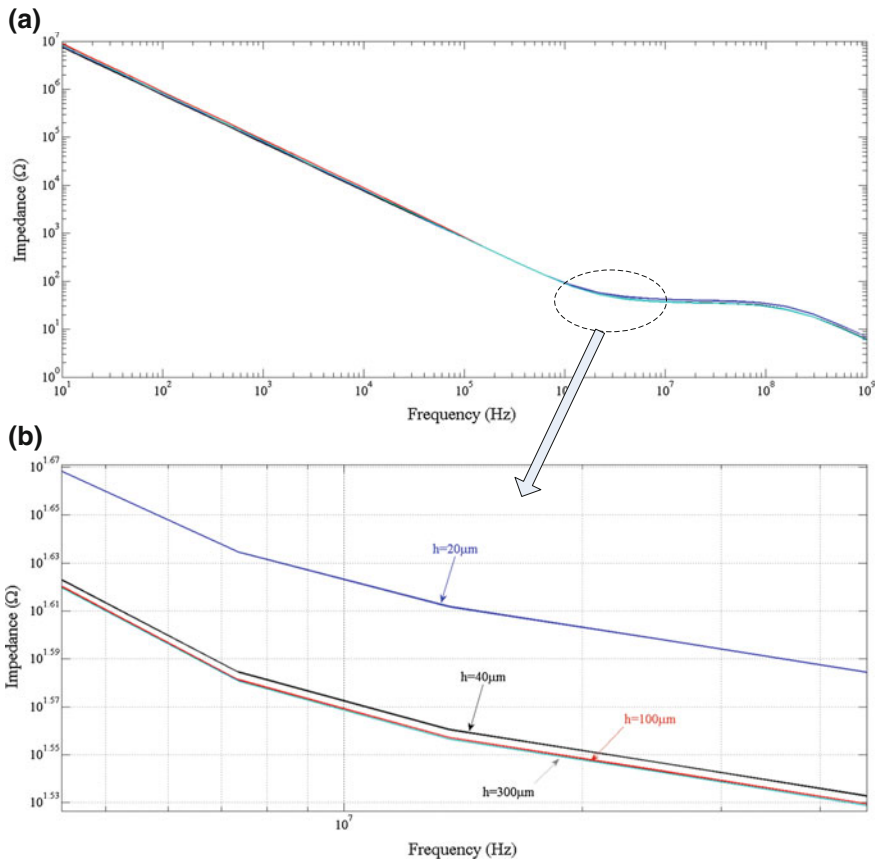


Fig. 18 **a** Impedance as a function of the frequency; **b** display zoomed in of **(a)**

4.1 Structuring of Layers and Masks Realization

The design is an important step in achieving our sensors. We define the necessary layers to complete the final system in three dimensions. They must also be compatible with available micro-manufacturing techniques.

The biological sample reservoir forms a square well (see Fig. 20) where a drop of biological sample for measure is deposited.

The realization of our sensors with interdigitate electrodes and their design using three layers (substrate, electrodes and reservoir) are presented on Fig. 21.

Once all the layers and geometrical sensor are defined, we realize the complete design of the sensor using CoventorWare[®]. The format “.GDS” is used as standard for the realization of masks.

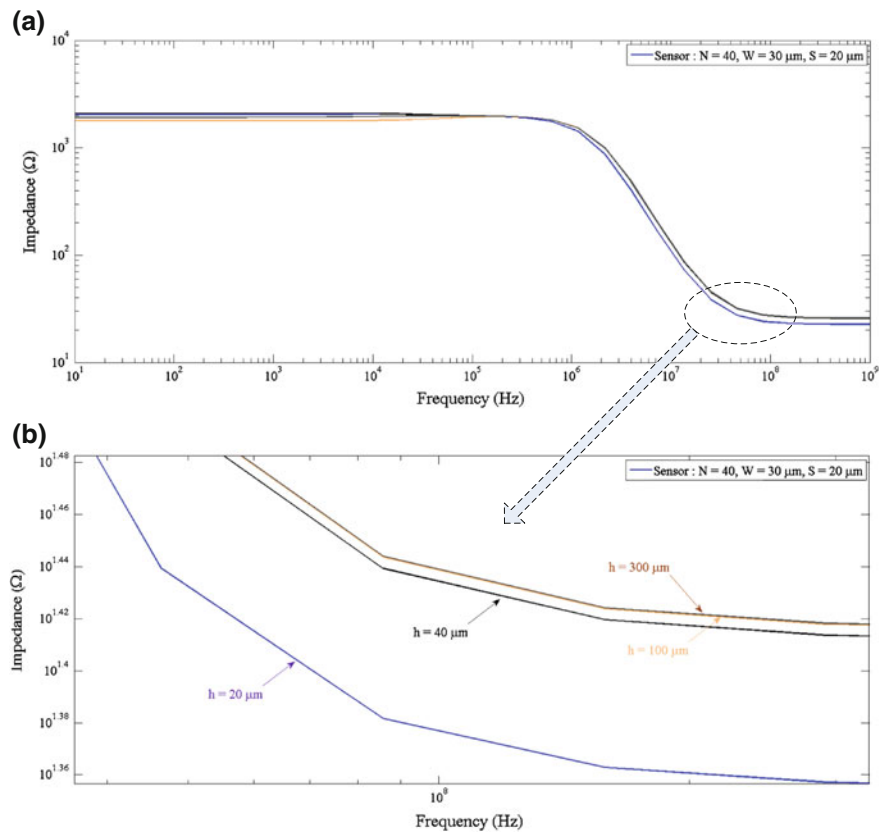


Fig. 19 **a** Impedance as a function of the frequency; **b** display zoomed in of (a)

Table 7 Parameters of the interdigital sensor manufacturing

Sensor	L (mm)	N	W (μm)	S (μm)	α	K_{cell} (m ⁻¹)
1	2	40	30	20	0.6	21.8
2	2	20	60	40	0.6	44.74
3	2	50	12	28	0.3	28.5
4	2	40	15	35	0.3	35.8
5	2	40	40	10	0.8	15.1

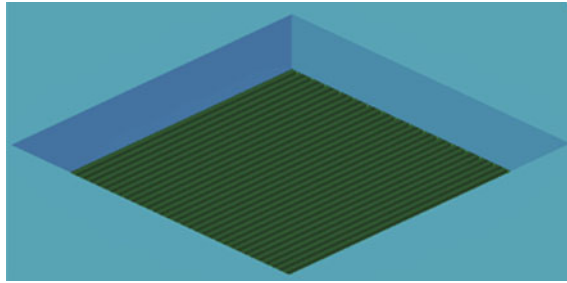


Fig. 20 Biological sample reservoir

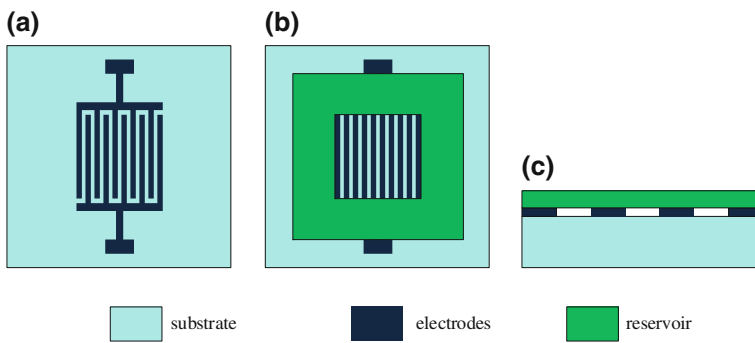


Fig. 21 Schematic representation of the layers. **a** The electrodes deposited on the substrate; **b** the reservoir layer deposited on the substrate carrying the electrodes; **c** the sensors consist of three layers

4.2 Manufacturing Process

Steps to fabricate a sensor are shown in Fig. 22:

- (a) The glass sample is first hand cleaned, with ultrasounds, hanging 10 min with a solution of NaOH, 10 min with a cleaner (RBS), 10 min with acetone then rinsed with isopropanol.
- (b) Deposit of a layer of catcher of tantalum about 10 nm then 150 nm of platinum by cathodic pulverizing.
- (c) Deposit of a layer of positive resin (S1813) by spreading with a spinner (SPIN COATING). With a positive resin, the parts exposed to UV radiation become more soluble and disappear during the development. The sample is placed on a heating plate to evaporate the solvent of the resin. We obtain a solid layer.
- (d) Exposure to the radiation UV
- (e) Development of the resin with a solvent (here the MF319). Only the parts of the resin which were not exposed to UV radiation resist the solvent. We obtain the negative of electrodes.

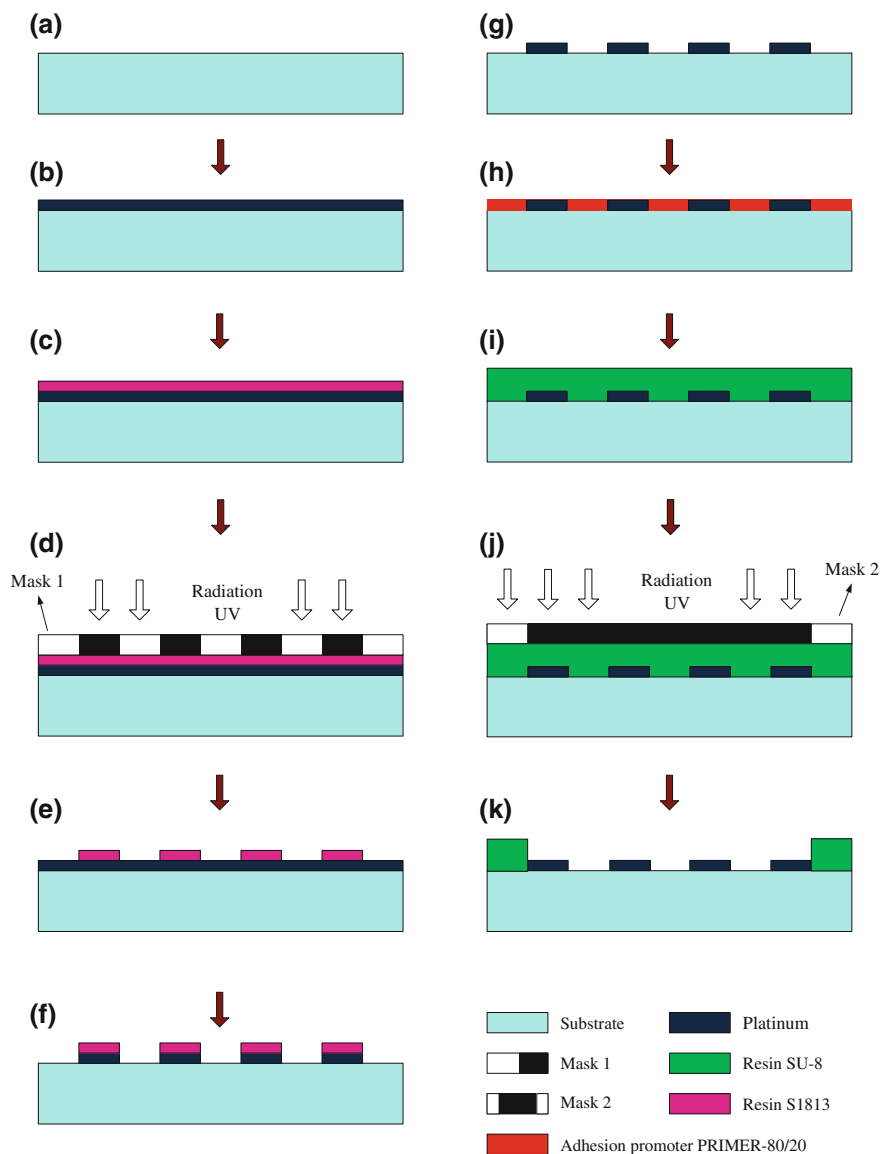


Fig. 22 Realization steps of our sensors. **a** Glass sample, **b** Deposition of the metal layer (150 nm platinum on 10 nm Tantalum), **c** Deposit of a resin layer S1813, **d** Exposure to radiation UV, **e** Development of resin S1813, **f** Platinum etching, **g** Removal of the photosensitive resin, **h** Coating the adhesion promoter and evaporation, **i** Deposit of a resin layer SU-8, **j** Exposure to radiation UV, **k** Development of resin SU-8

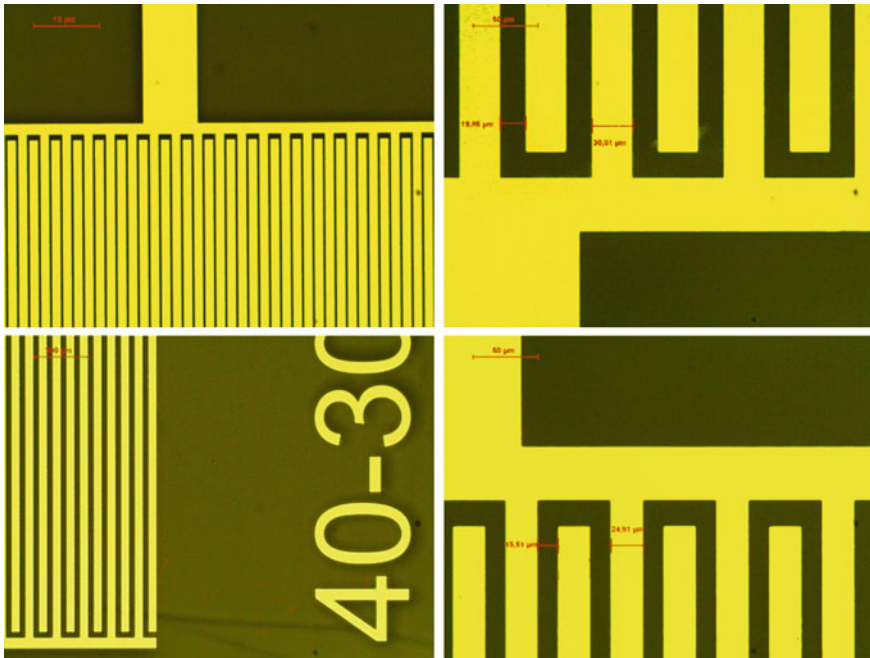


Fig. 23 Structures of the electrodes after the realization

- (f) The next step is the ion etching. The platinum electrodes are etched by an etching machine (Ionic beam etch – the IBE 4 Wave). A plasma is created, and the present ions in this plasma are accelerated towards the sample to come to pulverize the surface. The resin also is etched during the process, but its thickness is rather big to resist during the etching of the platinum.
- (g) After etching the rest of the resin (S1813) is removed with acetone.
- (h) Coating of the sample with an adhesion promoter (primer MMC 80/20). Once spread and evaporated on a heating plate, we can consider that the promoter does not form a layer unlike to a resin.
- (i) Depositing a layer of negative resin (SU-8) in the same way as in the step c). In the case of a positive resin, the part exposed to the radiation UV will become more resistant in solvents.
- (j) Exposure to the radiation UV
- (k) Development of the resin with a solvent (here the MF319). Only the parts of the resin which were not exposed to radiation UV resist the solvent. We obtain the negative of electrodes. After development of the resin we obtain the shape of reservoir.

Figures 23 and 24 present the results of the realization of our electrode sensors without reservoir.

Fig. 24 Image of the sensors after the realization without reservoir

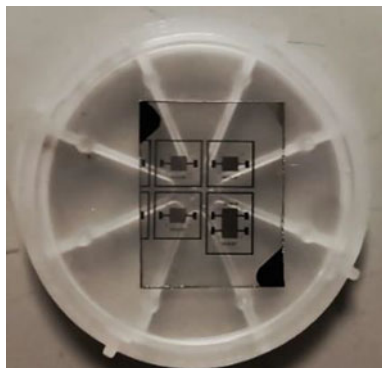
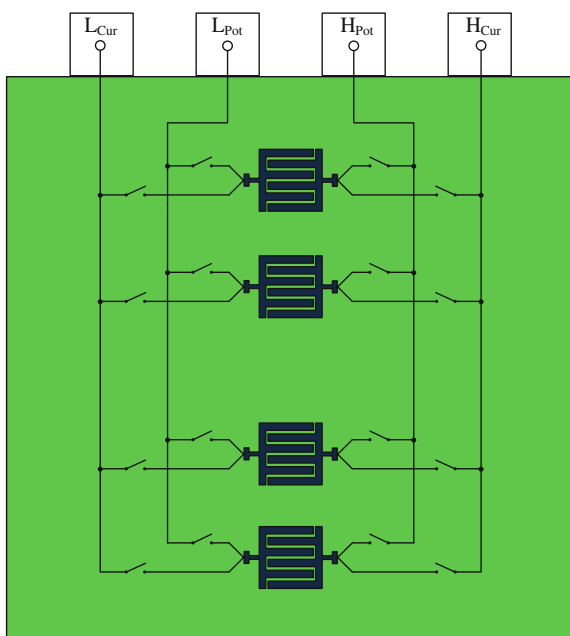


Fig. 25 Printed circuit board (PCB) to connect the sensor with a measuring instrument



We have designed a printed circuit board (PCB) to connect the sensor to the impedance meter (see Fig. 25). A four points method was used to make the impedance measurements. This method is used for the characterization of biological medium at frequencies below 100 MHz. It permits to eliminate the problems related to the impedance interface. This method requires the measurement of the current through the biofluids and the voltage at these terminals (Figs. 26 and 27).

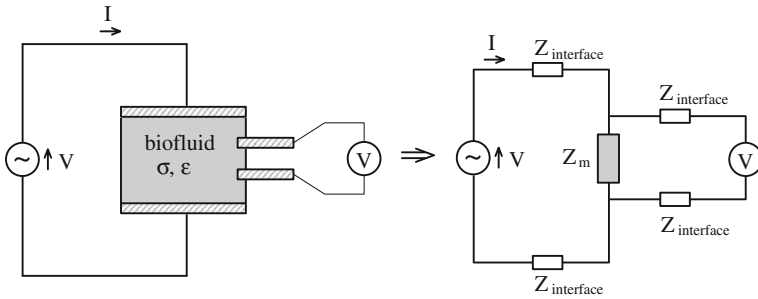
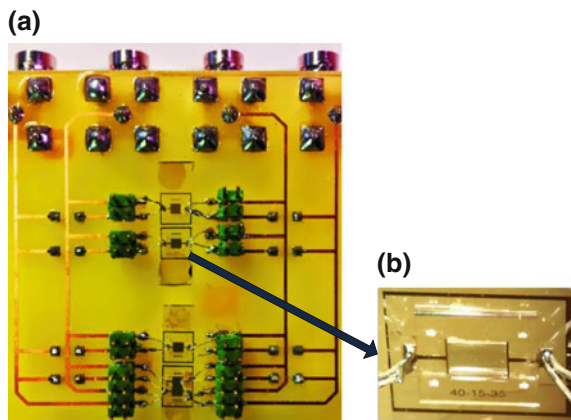


Fig. 26 The method of 4 points

Fig. 27 Photo of the micro-sensor (b) connected to the PCB (a)



5 Experimental Measurement

The experimental device consists on the following elements (Fig. 28):

- A drop of the sample solution with a conductivity of 12.88 mS/cm placed directly on the sensor (Figs. 29 and 30).
- A micropipette (Socorex Micropipette Acura 825) is used to add or remove the fluid volume.
- A thermometer to measure the ambient temperature.
- A microscope to observe the position of the liquid volume.
- A current amplifier HF2TA that converts 2 input currents to output voltages in a frequency range up to 50 MHz. This device is an active probe which can be conveniently placed close to the measurement setup. It supports most applications where a current must be converted to a voltage. The advanced design of the HF2TA ensures stability and a smooth operation over the entire frequency range. The HF2TA transimpedance current amplifier with the HF2 Series signal

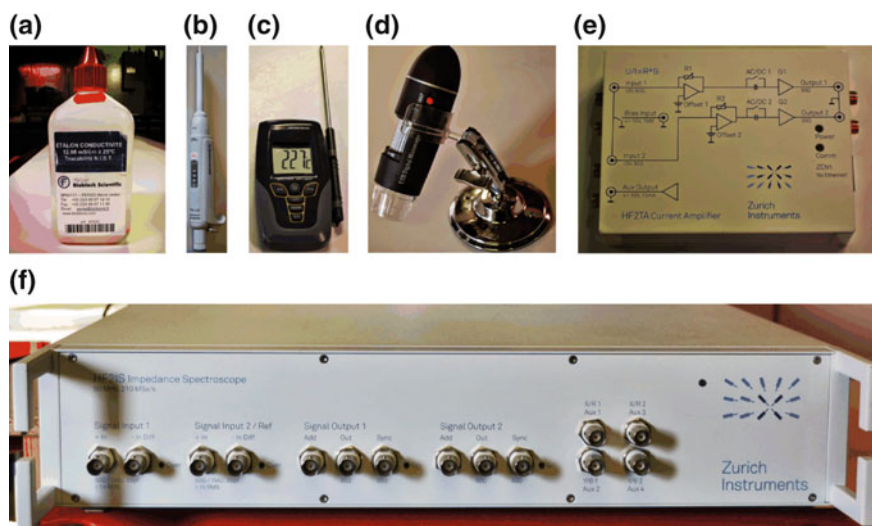


Fig. 28 Element of empirical measurement system: **a** the sample biofluids; **b** the micropipette; **c** the thermometer; **d** the microscope; **e** the current amplifier HF2TA; **f** the impedance spectroscopy HF2IS

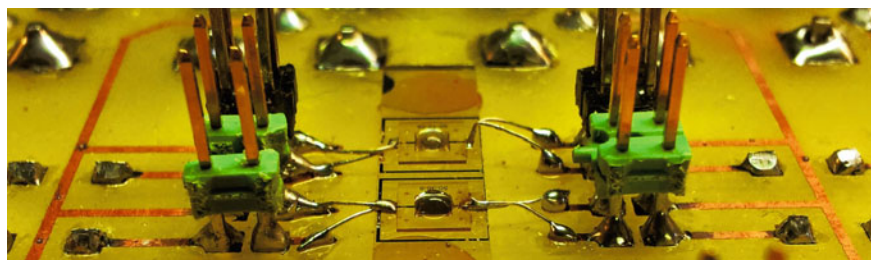


Fig. 29 A drop of the sample solution is placed directly on the sensor

analyzers allows for very high performance measurements and very low sensitivity to interferences.

- An impedance spectroscopy HF2IS covering a frequency range from 100 Hz to 10 MHz
- The biosensor with interdigitated electrodes.
- A computer for observation and data processing.

A sinusoidal signal (1 volt) is applied between the terminals of interdigitated electrodes and a frequency range of 10 Hz to 10 MHz is used for the experimental measurements.

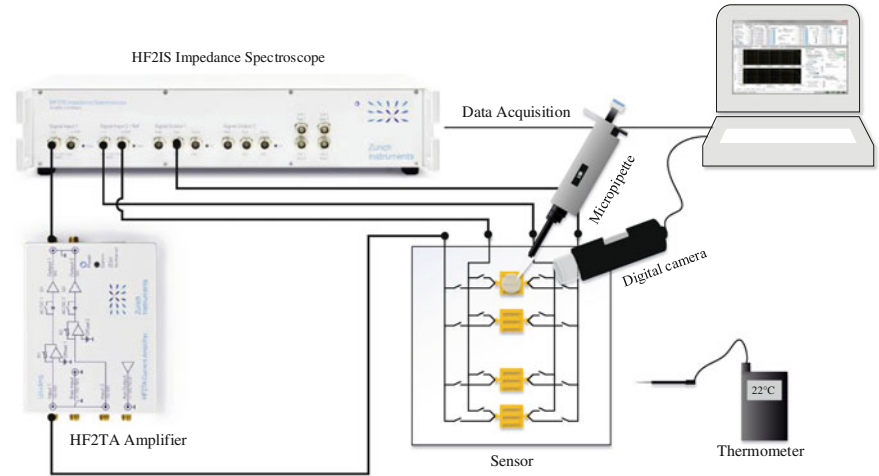


Fig. 30 Experimental set up for experimental measurements

In Fig. 31, we present the results of the impedance measurements as a function of the frequency for several types of sensors. The geometry of the sensor 1 is optimized, whereas the geometries of the sensor 2, 3, 4 and 5 are not optimized.

The results of experimental measurements indicated in Fig. 31 and Table 8 shows that the sensor 1 with a metal ratio of $\alpha = 0.6$ and the number of electrodes $N = 40$ has the lowest cutoff frequency. This confirms our theory and simulated results as presented above.

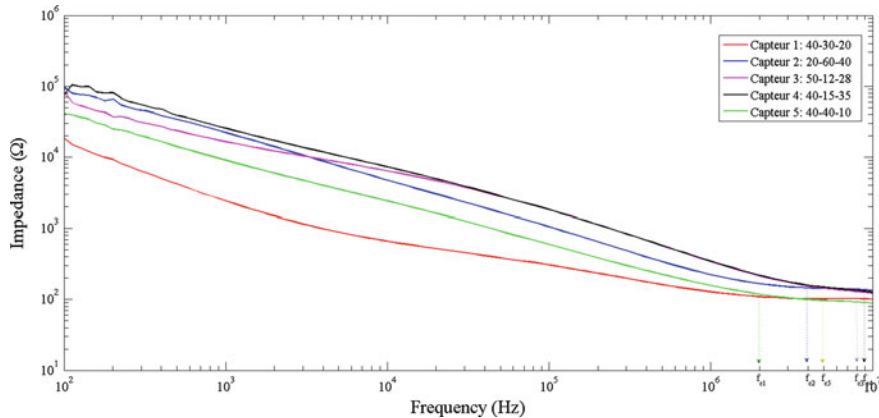


Fig. 31 Impedance amplitude as a function of the frequency

Table 8 Results of the experimental measurements

Sensor	L (mm)	N	W (μm)	S (μm)	α	f_{cut} (Hz)
1	2	40	30	20	0.6	1×10^6
2	2	20	60	40	0.6	4×10^6
3	2	50	12	28	0.3	8×10^6
4	2	40	15	35	0.3	9×10^6
5	2	40	40	10	0.8	5×10^6

6 Conclusion

In this work, we have proposed a new method to theoretically determine the parameters (relative permittivity, thickness and capacitance per unit area) of the double layer at the surface contact between the electrodes and the biological medium. Using an equivalent electrical circuit and the impedance formulae, we can estimate the capacitance per unit area C_0 according to the geometry (dimensions) of the sensor (N, L, W) and to the biological sample thickness. From this impedance we can deduce the values of the permittivity and the conductivity after having defined the cell factor K_{cell} .

We have described in detail the theoretical optimization method of the sensor’s geometric parameters with interdigitated electrodes to widen the useful frequency band and decrease the impedance interfaces. The optimization results allow us to choose the sensor with interdigitated electrodes existing the parameters: $\alpha = 0.6$, $N = 40$, $L = 20$ mm.

On the other hand, the thickness of the biological medium also influences the process of measure bio-impedance. So, it is necessary to ensure that a thickness of the biological medium is greater than 100 μm according to our optimization theory.

These results were defined theoretically in the first part, checked by simulation using CoventorWare[®], and also verified by measurement with a home-made experimental set up. The results are in good agreement with these three approaches.

References

1. K.S. Cole, H.J. Curtis, Electric impedance of the squid giant axon during activity. J. Gen. Physiol. **22**(5), 649–670 (1939)

2. H. Fricke, S. Morse, The electric capacity of tumors of the breast. J. Cancer Res. **10**, 340–376 (1926)

3. H. P. Schwan, Electrical properties of tissue and cell suspensions. Adv. Biol. Med. Phys. **5**, 147–209 (1957)

4. I. Giaever, C. Keese, Micromotion of mammalian cells measured electrically. Proc. Natl. Acad. Sci. USA **88**(17), 7896–7900 (1991)

5. D.A. Borkholder, *Cell Based Biosensors Using Microelectrodes.pdf* (Stanford University, Stanford, 1998)

6. M. Heuschkel, M. Fejtl, A three-dimensional multi-electrode array for multi-site stimulation and recording in acute brain slices. *J. Neurosci. Methods* **114**(2), 135–148 (2002)
7. R. Popovtzer, T. Neufeld, Electrochemical detection of biological reactions using a novel nano-bio-chip array. *Sens. Actuators B Chem.* **119**(2), 664–672 (2006)
8. J.S. Wei, Distributed capacitance of and acoustic surface. *IEEE J. Quantum Electron.* **13**(4), 152–158 (1977)
9. G. Alley, Interdigital capacitors and their application to lumped-element microwave integrated circuits. *Microw. Theory Tech. IEEE Trans.* **18**, 1028–1033 (1970)
10. P.R. Herczfeld, Special issue on applications of lightwave technology to microwave devices. *IEEE-INST Electr. Electron. Eng. INC* **38**(5), 465–466 (1990)
11. M. Ibrahim, J. Claudel, D. Kourtiche, M. Nadi, Geometric parameters optimization of planar interdigitated electrodes for bioimpedance spectroscopy. *J. Electr. Bioimpedance* **4**(1), 13–22 (2013)
12. T.-T. Ngo, H. Shirzadfar, D. Kourtiche, M. Nadi, A planar interdigital sensor for bio-impedance measurement: theoretical analysis, optimization and simulation. *J. Nano-Electron. Phys.* **6**(1), 1–7 (2014)
13. T. Ngo, H. Shirzadfar, A. Bourjilat, D. Kourtiche, M. Nadi, A method to determine the parameters of the double layer of a planar interdigital sensor. www-ist.massey.ac.nz (2014), pp. 2–4
14. M. Ibrahim, J. Claudel, D. Kourtiche, Physical and electrical modeling of interdigitated electrode arrays for bioimpedance spectroscopy. in *New Developments and Applications in Sensing Technology* (2011), pp. 169–189
15. W. Laureyn, D. Nelis, P. Van Gerwen, Nanoscaled interdigitated titanium electrodes for impedimetric biosensing. *Sens. Actuators B* 360–370 (2000)
16. L. Yang, Y. Li, C.L. Griffis, M.G. Johnson, Interdigitated microelectrode (IME) impedance sensor for the detection of viable *Salmonella typhimurium*. *Biosens. Bioelectron.* **19**(10), 1139–1147 (2004)
17. M. Varshney, Y. Li, Interdigitated array microelectrode based impedance biosensor coupled with magnetic nanoparticle-antibody conjugates for detection of *Escherichia coli* O157:H7 in food samples. *Biosens. Bioelectron.* **22**(11), 2408–2414 (2007)
18. R. Wang, Y. Wang, K. Lassiter, Y. Li, B. Hargis, S. Tung, L. Berghman, W. Bottje, Interdigitated array microelectrode based impedance immunosensor for detection of avian influenza virus H5N1. *Talanta* **79**, 159–164 (2009)
19. A.R. Mohd Syaifudin, S.C. Mukhopadhyay, P.-L. Yu, H.-S.M.J., C.-H. Chuang, V.J.D., Y.-W. Huang, Measurements and performance evaluation of novel interdigital sensors for different chemicals related to food poisoning. *IEEE Sens. J.* **11**(11), 2957–2965 (2011)
20. M. Da Silva, T. Sühnel, E. Schleicher, R. Vaibar, Planar array sensor for high-speed component distribution imaging in fluid flow applications. *Sensors* **7**, 2445 (2007)
21. F. Alexander, D.T. Price, S. Bhansali, Optimization of interdigitated electrode (IDE) arrays for impedance based evaluation of Hs 578T cancer cells. *J. Phys: Conf. Ser.* **224**, 012134 (2010)
22. T. Huang, J. Chou, T. Sun, and S. Hsiung, A device for skin moisture and environment humidity detection. *Sens. Actuators B* **134**, 206–212 (2008)
23. V. Kasturi, S.C. Mukhopadhyay, Estimation of property of sheep skin to modify the tanning process using interdigital sensors. *Lecture Notes in Electrical Engineering*, vol. 21 LNEE, pp. 91–110 (2008)
24. M. Mukhopadhyay, S.C. Yamada, S. Iwahara, Evaluation of near- surface material properties using planar mesh type coils with post-processing from neural network model. *Int. J. Electromagn. Nondestructive Eval.* **23**, 181–188 (2002)
25. M.I.S.C. Mukhopadhyay, S. Yamada, Inspection of electroplated materials—performance comparison with planar meander and mesh type magnetic sensor. *Int. J. Appl. Electromagn. Mech.* **15**, 323–329 (2002)
26. A. Choi, J. Park, H. Jung, Solid-medium-integrated impedimetric biosensor for real-time monitoring of microorganisms. *Sens. Actuators B Chem.* **137**, 357–362 (2009)

27. B. Pejic, R. De Marco, Impedance spectroscopy: Over 35 years of electrochemical sensor optimization. *Electrochim. Acta* **51**(28), 6217–6229 (2006)
28. R. Igreja, C.J. Dias, Analytical evaluation of the interdigital electrodes capacitance for a multi-layered structure. *Sens. Actuators A Phys.* **112**(2–3), 291–301 (2004)
29. C.R. Bowen, L.J. Nelson, R. Stevens, M.G. Cain, M. Stewart, Optimisation of interdigitated electrodes for piezoelectric actuators and active fibre composites. *J. Electroceramics* **16**(4), 263–269 (2006)
30. L. Wang, H. Wang, K. Mitchelson, Z. Yu, J. Cheng, Analysis of the sensitivity and frequency characteristics of coplanar electrical cell-substrate impedance sensors. *Biosens. Bioelectron.* **24**(1), 14–21 (2008)
31. T. Pajkossy, D.M. Kolb, Double layer capacitance of Pt(111) single crystal electrodes. *Electrochim. Acta* **46**(20–21), 3063–3071 (2001)
32. David A. Borkholder, *Cell Based Biosensors Using* (1998)
33. A. Bard, L. Faulkner, *Fundamentals and Applications* (1980)
34. R. Pradhan, A. Mitra, and S. Das, *Extended Stern Model* (2012), pp. 74–78
35. W. Olthuis, W. Streekstra, P. Bergveld, Theoretical and experimental determination of cell constants of planar-interdigitated electrolyte conductivity sensors. *Sens. Actuators B* **25**, 252–256 (1995)
36. B. Timmer, W. Sparreboom, W. Olthuis, P. Bergveld, A. van den Berg, Optimization of an electrolyte conductivity detector for measuring low ion concentrations. *Lab Chip* **2**(2), 121–124 (2002)
37. J.-F. Chateaux, *Conception et réalisation d'une cellule de caractérisation des tissus biologiques par spectroscopie de bioimpédance dans la gamme fréquentielle [100 Hz–1 MHz]. Application aux tissus osseux—Prise en compte de l'anisotropie* (Thèse de l'Université Henri Poincaré, Nancy I, 2000)
38. L. Bernard, Caractérisation électrique des tissus biologiques et calcul des phénomènes induits dans le corps humain par des champs électromagnétiques de fréquence inférieure au GHz ., Thèse de l'Ecole Centrale de Lyon, 2007
39. Ifac 2012, Calculation of the dielectric properties of body tissues in the frequency range 10 Hz–100 GHz. <http://niremf.ifac.cnr.it/tissprop/htmlclie/htmlclie/htmlclie.php>
40. O. Linderholm, Two-dimensional microimpedance imaging for cell culture monitoring, vol. 3604 (2006)
41. C. Veyres, V.F. Hanna, Extension of the application of conformal mapping techniques to coplanar lines with finite dimensions. *Int. J. Electron.* **48**(1), 47–56 (1980)
42. V. 2010, *Coventor Ware® ANALYZER* (2010)



<http://www.springer.com/978-3-319-21670-6>

Next Generation Sensors and Systems

Mukhopadhyay, S.C. (Ed.)

2016, XII, 330 p. 251 illus., 178 illus. in color.,

Hardcover

ISBN: 978-3-319-21670-6